

Fume Model for Gas Metal Arc Welding

Metal evaporation and condensation calculations predict fume formation rate for DC-positive operation in globular and spray modes

BY C. J. REDDING

ABSTRACT. This paper describes changes to a previous model for calculating fume formation rate in mild steel gas metal arc welding (GMAW). The changes attempt to produce a more theoretically based model. They include calculation of droplet falling time in place of empirical values, mass transfer rate from droplet to plasma in place of the Langmuir equation for evaporation into a vacuum, and fraction metal vapor condensing to base metal, which varies with parameters in place of a fixed 90% condensation value. The model is for DC electrode positive (DCEP) operation in the globular and spray modes. It has been applied to an experimental data set, used in the previous model, for a 1.2-mm-diameter (0.047-in.) mild steel welding wire. The new model is shown to be a poorer predictor than the previous model. The new model also predicts Fe to Mn ratio in the fume from which concentrations can be estimated. Fe concentration is underestimated and Mn concentration is overestimated with greater divergence from experimental results at the higher currents.

Introduction

Welding Fume and Health Risks

Worldwide, industry lays down an estimated one million tons of weld metal annually. Based on an average fume production of 0.5% of weld metal, an estimated five thousand tons of fume are produced annually. Some of this fume is breathed in by the welder and can affect health. Effects on the welder include irritation of the lining of the lungs and metal fume fever. Studies have indicated a slightly increased prevalence of lung cancer (Refs. 1, 2) and asthma (Ref. 3) as a result of welding work. A way of predicting fume formation rate (FFR) and fume composition in a given situation may aid occupational hygienists in assessing fume exposure risk, although the

link between emission and exposure is not clear. Prediction of FFR as a function of welding parameters may also aid industries in selecting lower fume operating conditions. An understanding of how fume is formed may aid welding consumable manufacturers in developing lower fume products and processes.

Fume Formation Rate Models

Prediction models can be empirically or theoretically based or an intermediate between the two (semiempirical). This paper describes an intermediate model. Fume is micron and submicron solid particles that are largely metal oxides. In globular and spray modes, it forms mainly by evaporation of metal from droplets at a temperature of approximately 2500 K. There is some evaporation from the weld pool. Fume can also be formed through bursting of gas bubbles in droplets and from droplets thrown out of the arc region that rapidly oxidize in air (spatter). Most of the metal vapor is thought to condense without forming fume but some leaves the arc region and reacts with oxygen to form metal oxide fume. Only fume formed by evaporation from droplets forming on the welding wire tip and falling through the arc was considered here.

Model Development

The model described draws on two semiempirical models for FFR: the first, referred to here as the Deam Model (Ref.

4), and the second, referred to here as the Dennis Model (Ref. 5). Both models rely on results of theoretical work by Haidar (Ref. 6). The models predict droplet temperature, calculate metal evaporation from the droplets and subsequent condensation to the base metal, and result in prediction of metal vapor to fume rate. The aim of the New Model was to produce a procedure that improved modeling of the system and required fewer difficult-to-measure inputs. To be generally useful, a model should be able to predict FFR using commonly measured welding parameters combined with information on the welding wire supplied by the manufacturer. The Dennis Model, in addition to physical property data inputs, required welding current, welding wire feed rate, droplet rate, electrode extension, and arc length. Experiments to test the Dennis Model used an argon-based shielding gas containing 5% CO₂ and 2% O₂. Standoff distance was 35 mm (1.378 in.) and arc length was 5 mm (0.197 in.), giving an electrode extension of 30 mm (1.181 in.). Arc length is not a commonly or easily measured quantity in many welding situations, and the New Model does not require it to be measured.

Note: In the text, linear dimensions for Tables 3 and 4 are given in millimeters and inches. The model equations use SI units, so for calculation purposes, dimensions must be in meters, as specified in Table 1.

Method

A description of the Dennis Model is given, followed by comments on changes made in the New Model. Details on the equations are then given. The New Model has been applied to the Dennis Model experimental data set (Ref. 5) and the resulting droplet temperatures and FFRs compared with the Dennis Model results.

The Dennis Model

Droplet Temperature

Droplet temperature was calculated using an energy balance on the welding

KEY WORDS

DCEP
Deam Model
Dennis Model
Fume Formation Rate
Gas Metal Arc Welding
Welding Fume

C. J. REDDING is with the Metal Fume Research Unit, Department of Environmental Science, University of Bradford, Bradford, UK.

Table 1 — Definitions of Symbols and Conversion Factors

| | | |
|--------------|--|--|
| A_{dp} | droplet projected area | [m ²] (1550 in. ²) |
| A_{ds} | droplet surface area | [m ²] (1550 in. ²) |
| A_w | welding wire cross-sectional area | [m ²] (1550 in. ²) |
| C_p | welding wire and droplet specific heat capacity | [J.kg ⁻¹ .K ⁻¹](0.239 x 10 ⁻³ Btu.lb ⁻¹ °F ⁻¹) |
| C_{pp} | plasma specific heat capacity | [J.kg ⁻¹ .K ⁻¹](0.239 x 10 ⁻³ Btu.lb ⁻¹ °F ⁻¹) |
| d_d | droplet diameter | [m](39.37 in.) |
| d_w | welding wire diameter | [m](39.37 in.) |
| D_{AB} | mass diffusivity element A through element B | [m ² .s ⁻¹](1550 in. ² .s ⁻¹) |
| e | charge on an electron | [C] |
| E_i | mass evaporated for element i | [kg](2.205 lb) |
| f | friction coefficient | [] |
| F_d | force on droplet | [N](0.225 lbf) |
| g | acceleration due to gravity | [m.s ⁻²](0.03937 in. ² .s ⁻²) |
| h | convective heat transfer coefficient | [W.m ⁻² .K ⁻¹](0.176 Btu.h ⁻¹ .ft ⁻² .°F ⁻¹) |
| H_{fusion} | welding wire latent heat of fusion | [J.kg ⁻¹](0.430 x 10 ⁻⁶ Btu.lb ⁻¹) |
| H_L | welding wire tip volumetric heat content | [J.m ⁻³](0.268 x 10 ⁻⁶ Btu.ft ⁻³) |
| H_{vFe} | latent heat of vaporization Fe | [J.kg ⁻¹](0.430 x 10 ⁻⁶ Btu.lb ⁻¹) |
| H_{vMn} | latent heat of vaporization Mn | [J.kg ⁻¹](0.430 x 10 ⁻⁶ Btu.lb ⁻¹) |
| i | element Fe or Mn | [] |
| I | current | [A] |
| j_w | welding wire current density = I/A_w | [A.m ⁻²](0.645 x 10 ⁻³ A.in. ²) |
| k | Boltzman's constant | [J.K ⁻¹](0.527 x 10 ⁻³ Btu.°F ⁻¹) |
| k_{ci} | mass transfer coefficient element i | [m.s ⁻¹](39.37 in. ² .s ⁻¹) |
| k_{Tp} | plasma thermal conductivity | [W.m ⁻¹ .K ⁻¹](0.578 Btu.h ⁻¹ .ft ⁻¹ .°F ⁻¹) |
| l_{mix} | metal vapor into shielding gas mixing length = $d_w/2$ | [m](39.37 in.) |
| L | electrode extension | [m](39.37 in.) |
| L_a | arc length | [m](39.37 in.) |
| m_d | droplet mass | [kg](2.205 lb) |
| M_{FFR} | metal vapor to fume rate | [kg.s ⁻¹](2.205 lb.s ⁻¹) |
| M_i | atomic mass element i | [kg.mol ⁻¹](2.205 lb.mol ⁻¹) |
| M_{VGR} | metal vapor generation rate | [kg.s ⁻¹](2.205 lb.s ⁻¹) |
| μ_f | plasma viscosity at film temperature | [N.s.m ⁻²](0.6672 lb.ft ⁻¹ .s ⁻¹) |
| N_u | Nusselt number = hd_d/k_{Tp} | [] |
| P_i | pure vapor pressure element i | [N.m ⁻²](0.145 x 10 ⁻³ lbf.in. ⁻²) |
| Pr | Prandtl number = $\mu_f C_{pp}/k_{Tp}$ | [] |
| Q_{Con} | convection energy transfer | [J](0.948 x 10 ⁻³ Btu) |
| Q_{Evap} | evaporative energy loss | [J](0.948 x 10 ⁻³ Btu) |
| Q_{rad} | radiation energy transfer | [J](0.948 x 10 ⁻³ Btu) |
| Q_{res} | resistive heating in droplet | [J](0.948 x 10 ⁻³ Btu) |
| R | Universal gas constant | [J.mol ⁻¹ .K ⁻¹](0.527 x 10 ⁻³ Btu.mol ⁻¹ .°F ⁻¹) |
| Re | Reynolds number = $\rho U_{pdd}/\mu_f$ | [] |
| ρ_d | droplet density | [kg.m ⁻³](62.4 x 10 ⁻³ lb.ft ⁻³) |
| ρ_f | plasma density at film temperature | [kg.m ⁻³](62.4 x 10 ⁻³ lb.ft ⁻³) |
| ρ_{vi} | vapor density element i | [kg.m ⁻³](62.4 x 10 ⁻³ lb.ft ⁻³) |
| ρ_w | welding wire density | [kg.m ⁻³](62.4 x 10 ⁻³ lb.ft ⁻³) |
| S_c | Schmidt number = $\mu_f/(r_f D_{AB})$ | [] |
| S_h | Sherwood number = $k_c d_d/D_{AB}$ | [] |
| σ_d | droplet resistivity | [Ω.m](39.37 Ω.in.) |
| t | time period | [s] |
| t_{fall} | droplet falling time | [s] |
| T_a | ambient temperature | [K] |
| T_d | droplet mean temperature | [K] |
| T_{ds} | droplet surface temperature | [K] |
| T_f | film temperature = $(T_p - T_{ds})/2$ | [K] |
| T_m | welding wire melting temperature | [K] |
| T_p | plasma (arc) temperature | [K] |
| u_w | welding wire velocity | [m.s ⁻¹](39.37 in. ² .s ⁻¹) |
| U_o | shielding gas velocity at nozzle outlet | [m.s ⁻¹](39.37 in. ² .s ⁻¹) |
| U_p | plasma velocity = $3809u_w$ | [m.s ⁻¹](39.37 in. ² .s ⁻¹) |
| V_a | anode potential | [V] |
| V_{wf} | droplet material work function potential | [V] |
| ω | droplet transfer frequency | [s ⁻¹] |
| x_i | mass fraction element i in droplet | [] |
| X_i | mole fraction element i in droplet | [] |

wire extension and droplet forming at its tip. Current flowing in the welding wire extension heats it up. Electrons transferring from the arc provide further energy

and this results in melting of the welding wire and an increase in its temperature above the melting point. The molten welding wire forms a droplet at the weld-

ing wire tip. A mild steel welding wire was studied and Fe and Mn evaporation considered separately. From the initial energy balance the initial droplet temperature was found.

Evaporation from Forming Droplet

From the droplet temperature, the initial evaporation rate was calculated using the Langmuir equation for evaporation into a vacuum. At the welding wire tip the droplet grows, receiving mass from the welding wire and losing it by evaporation. Mass balances over small time intervals were integrated to give the total mass loss over droplet formation time. Incremental energy balances accounting for resistance heating in the droplet and evaporative energy loss were also performed and the droplet temperature change calculated. Radiation and convection energy transfers were estimated, found to be small compared to other energy transfers, and were ignored.

Evaporation from Falling Droplet

Eventually the droplet detaches and no longer receives mass from the welding wire being fed in. The energy exchange situation also changes. Separate calculations were made for the falling droplet. Droplet falling time was estimated using arc length measurement together with experimental data for droplet velocity (Ref. 7). The data was applicable to a 5-mm (0.047-in.) arc and, although mild steel welding wire size was not explicitly given, it can be implied to have been 1.6 mm (0.063 in.) rather than the 1.2 mm (0.047 in.) used in the Dennis Model experiments. Current and welding wire velocity combinations were also different, so using the data was not ideal.

Suitability of Langmuir Equation

The Dennis Model assumed oxidation of metal vapor close to the droplet surface resulted in evaporation (oxidation-enhanced evaporation) close to that predicted by the Langmuir equation. This has been shown to be the case for Fe evaporating into an oxidizing atmosphere (Ref. 8), but the experiments were performed at much lower temperatures than those encountered in the arc. In the case of Mn, the oxidation-enhanced rates were less than 10% of the Langmuir rate. Doubt was expressed (Ref. 5) that FeO could exist at the temperatures encountered near the droplet surface. Fe initially forms FeO, which boils at 2700 K and decomposes at 3400 K. The droplet surface would be between about 2000 and 3000 K, with the arc plasma between 6000 and

20,000 K or higher. The Dennis Model used mean droplet temperature in the calculations, although droplet surface temperature would be expected to be higher than this.

The New Model

The New Model replaces the Langmuir equation with calculation of convective mass transfer coefficients for Fe and Mn and, thence, evaporation rates. Radiation and convective energy transfers were estimated and incorporated into the energy balances. In calculations, droplet surface temperature was used in place of mean temperature. Droplet falling time was estimated by calculating arc length from stand-off, welding wire feed velocity, and current using an equation for electrode extension derived from Halmøy's paper (Ref. 9). This was combined with a calculation of droplet acceleration resulting from gravity and drag force due to the high-velocity plasma flowing around the droplet. The plasma velocity was estimated from an equation used in the Deam Model. It applies to a 1.2-mm-diameter (0.047-in.) welding wire. Condensation to the base metal was estimated using the method described in the Deam Model. The method is based on potential flow and incorporates shielding gas velocity and metal vapor density at the droplet surface. Details of equations are given below. Definitions of symbols used, with units and conversion factors, are given in Table 1. Values of physical properties, constants, and parameters are given in Table 2.

Droplet Temperature

The initial mean droplet temperature as a new drop starts to form after the previous one has detached from the welding wire tip was calculated using the Dennis Model initial energy balance equation, which follows:

$$\begin{aligned}
 & u_w A_w \rho_w \left\{ C_p (T_d - T_a) + H_{fusion} \right\} t \\
 & = H_L u_w A_w t \\
 & + \left(V_{wt} + V_a + \left(\frac{3k}{2e} \right) (T_p - T_d) \right) It \quad [K] \quad (1)
 \end{aligned}$$

The term on the left-hand side represents the energy absorbed in raising the temperature of the welding wire fed into the arc from ambient temperature to the mean droplet temperature and includes the heat of fusion. The energy was provided by resistance heating in the welding wire extension (first term on right-hand side) plus electron condensation heating comprising work function potential plus anode potential plus kinetic energy loss per coulomb multiplied by the coulombs of charge as electrons condensing (It).

Table 2 — Values of Physical Properties, Constants, and Parameters

| | | | |
|--------------|--|------------|--|
| A_w | $1.13 \times 10^{-6} \text{ [m}^2\text{]}$ | M_{Mn} | $54.9 \times 10^{-3} \text{ [kg.mol}^{-1}\text{]}$ |
| C_p | $753 \text{ [J.kg}^{-1}\text{.K}^{-1}\text{]}$ | μ_f | $0.172 \times 10^{-3} \text{ [N.s.m}^{-2}\text{]}$ |
| C_{pp} | $593 \text{ [J.kg}^{-1}\text{.K}^{-1}\text{]}$ | P_r | 0.622 [] |
| d_w | $1.20 \times 10^{-3} \text{ [m]}$ | R | $8.314 \text{ [J.mol}^{-1}\text{.K}^{-1}\text{]}$ |
| D_{FeAr} | $2.89 \times 10^{-3} \text{ [m}^2\text{.s}^{-1}\text{]}$ | ρ_f | $78.1 \times 10^{-3} \text{ [kg.m}^{-3}\text{]}$ |
| D_{MnAr} | $2.90 \times 10^{-3} \text{ [m}^2\text{.s}^{-1}\text{]}$ | ρ_w | $7.70 \times 10^3 \text{ [kg.m}^{-3}\text{]}$ |
| e | $0.160 \times 10^{-18} \text{ [C]}$ | σ_d | $1.32 \times 10^{-6} \text{ }\Omega\text{.m]}$ |
| g | $9.81 \text{ [m.s}^{-2}\text{]}$ | T_a | 293 [K] |
| H_{fusion} | $247 \times 10^3 \text{ [J.kg}^{-1}\text{]}$ | T_f | $6.25 \times 10^3 \text{ [K]}$ |
| H_{vFe} | $6.54 \times 10^6 \text{ [J.kg}^{-1}\text{]}$ | T_m | $1.81 \times 10^3 \text{ [K]}$ |
| H_{vMn} | $4.31 \times 10^6 \text{ [J.kg}^{-1}\text{]}$ | T_p | $10.0 \times 10^3 \text{ [K]}$ |
| k | $13.8 \times 10^{-24} \text{ [J.mol}^{-1}\text{.K}^{-1}\text{]}$ | U_o | $3.90 \text{ [m.s}^{-1}\text{]}$ |
| k_{Tp} | $0.164 \text{ [W.m}^{-1}\text{.K}^{-1}\text{]}$ | V_a | 1.00 [V] |
| l_{mix} | $0.600 \times 10^3 \text{ [m]}$ | V_w | 4.18 [V] |
| M_{Fe} | $55.9 \times 10^{-3} \text{ [kg.mol}^{-1}\text{]}$ | | |

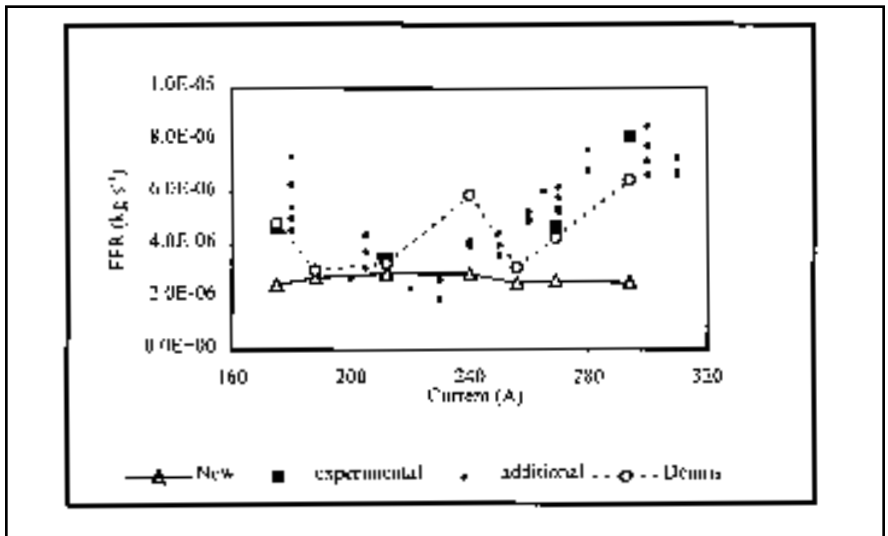


Fig. 1 — FFR against current: experimental values and the Dennis Model predictions from Ref. 5 with the New Model predictions added.

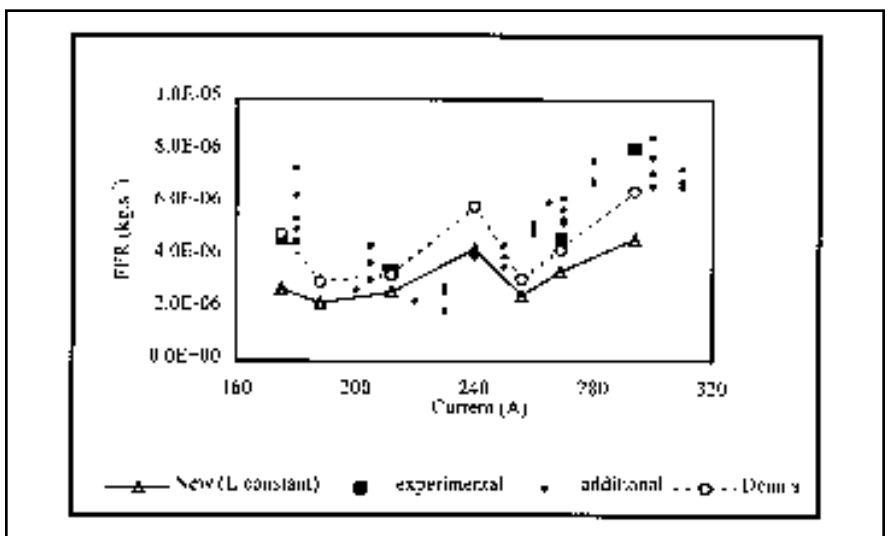


Fig. 2 — FFR against current: experimental values from Ref. 5 with New Model predictions assuming constant electrode extension and arc length.

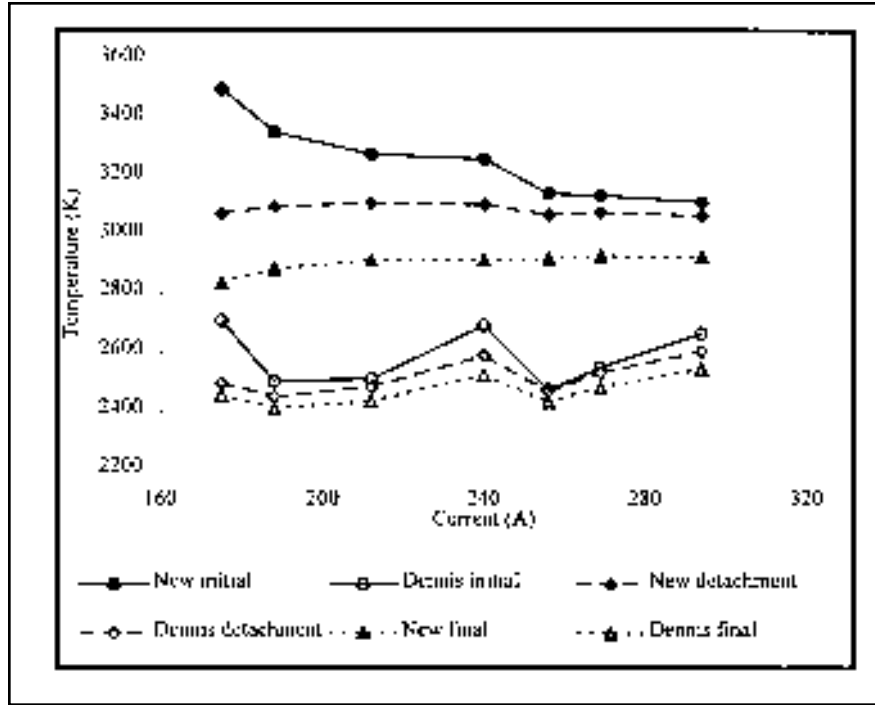


Fig. 3 — Droplet temperatures predicted by the Dennis and New Models.

The analysis only applies to electrode positive operation, which is the most common form of GMAW. Resistance heating in the welding wire was calculated using a method described by Halmøy (Ref. 9). The energy content per unit volume at the end of the electrode extension as a result of resistance heating in the welding wire, H_L , was given by a second order polynomial curve fit to Halmøy's data for Union K56 Si-Mn steel solid welding wire (Ref. 5).

$$H_L = 1.69 \times 10^7 + 2.232 \times 10^{-7} \left(\frac{Lj_w^2}{u_w} \right) + 5.98 \times 10^{-23} \left(\frac{Lj_w^2}{u_w} \right)^2 \quad [J.m^{-3}] \quad (2)$$

The droplet surface temperature was given by

$$T_{ds} = 2(T_d - T_m) + T_m \quad [K] \quad (3)$$

This was derived from the assumption the mean droplet temperature was midway between droplet melting point and droplet surface temperature as in the Deam Model. The incremental time period chosen for the forming droplet was $\frac{1}{100}$ th of the formation time where the formation time was given by the inverse of

the droplet rate ($1/\omega$). Over this incremental time period, the volume of welding wire that flowed into the droplet, expressed as volume at droplet temperature, was

$$\text{Incremental volume} = u_w A_w \rho_w / (\rho_d \cdot 100\omega) \quad [m^3] \quad (4)$$

From this volume, a droplet surface area was calculated assuming a spherical droplet. Droplet density was evaluated as a function of droplet temperature using an equation fitted to density data. The density data was for a 1.4% Mn in Fe alloy calculated using an estimation method supplied by the U.K. National Physical Laboratory. The Dennis Model used an equation derived from density data for liquid 304 stainless steel (Ref. 10). There was not a lot of difference between the densities calculated using the two different equations, and model results are fairly insensitive to small changes in density.

$$\rho_d = 8363.2 - (T_d) + 6.559 \times 10^{-5} (T_d^2) \quad [kg.m^{-3}] \quad (5)$$

Droplet Resistance Heating

Resistance heating in the droplet was calculated using a Dennis Model equa-

tion that assumed a constant resistance, molten metal cylinder of the same diameter as the droplet at detachment, ignoring evaporation mass loss, and of a length equal to the diameter of the droplet at any given time. Current density was assumed constant with position at a given time. This is a very simple approximation for what is a complex situation. In reality, the resistivity, conductor cross section, and current density in a droplet varies with position and is dependent both on the area covered by the arc and droplet shape. The resulting equation for resistance heating integrated over the time period t_1 to t_2 was

$$Q_{Res} = \sigma_d I^2 \left(\frac{3}{2\pi} \right) \left(\frac{4\pi\rho_d}{u_w A_w \rho_w} \right)^{1/3} \omega^{2/3} (t_2^{4/3} - t_1^{4/3}) \quad [J] \quad (6)$$

Radiation Energy Transfer

Radiation energy loss from the droplet over a given time increment was estimated using the equation

$$Q_{Rad} = 5.67 \times 10^{-8} A_{ds} (0.29) (T_{ds}^4) (1/100\omega) \quad [J] \quad (7)$$

where 5.67×10^{-8} [W/m²/K⁴] is the Stefan-Boltzman constant and 0.29 is the emissivity of the molten metal surface. The equation assumes no radiation received from the arc by the droplet, *i.e.*, arc emissivity is zero. The estimation of arc emissivity is complex. One estimate for an argon plasma arc was 0.012 (Ref. 11), but Welty, Wicks, and Wilson (Ref. 12) state inert gases and diatomic gases of symmetrical composition, such as O₂, can be considered transparent to thermal radiation. They also state polyatomic gases such as CO₂ absorb and emit radiation. Shielding gases often contain CO₂, so radiation loss from the droplet should decrease as CO₂ shielding gas content increases due to the droplet receiving more radiation from the arc; this, in turn, should increase metal evaporation rate.

Convection Energy Transfer

Convective energy transfer from the arc to the droplet was calculated from the equation

$$Q_{Con} = h A_{ds} (T_p - T_{ds}) (1/100\omega) \quad [J] \quad (8)$$

h is the convective heat transfer coeffi-

Table 3 — Experimental Data Set from Ref. 2

| | | | | | | | | |
|---|---|-------------------------|-------|-------------------------|-------|-------|-------------------------|-------------------------|
| Typical welding wire composition (mass %) | C | Mn | Si | Fe | | | | |
| | 0.1 | 1.4 | 0.9 | 97.6 | | | | |
| Welding wire diameter | :1.2 mm (0.047 in.) | | | | | | | |
| Standoff | :35 mm (1.378 in.) | | | | | | | |
| Arc length | :5 mm (0.197 in.) | | | | | | | |
| Welding polarity | :DC electrode positive | | | | | | | |
| Shielding gas composition | :93%Ar, 5%CO ₂ , 2%O ₂ | | | | | | | |
| Shielding gas flow rate | :7.8 x 10 ⁻⁴ m ³ .s ⁻¹ (1.66 ft ³ .min. ⁻¹) | | | | | | | |
| Experimental test | 1 | 2 | 3 | 4 | 5 | 6 | 7 | |
| Droplet rate (ω) | [s ⁻¹] | 33.4 | 80.9 | 130.7 | 122.4 | 158.7 | 182.8 | 172.4 |
| Wire velocity (u_w) | [m.s ⁻¹] | 0.091 | 0.108 | 0.129 | 0.148 | 0.175 | 0.185 | 0.207 |
| Current (I) | [A] | 175 | 188 | 212 | 240 | 256 | 269 | 294 |
| FFR | [kg.s ⁻¹] | 4.67 x 10 ⁻⁶ | | 3.45 x 10 ⁻⁶ | | | 4.68 x 10 ⁻⁶ | 8.15 x 10 ⁻⁶ |

cient obtained from a relationship between the Nusselt number, $N_u = hd_d/k_p$; the Reynolds number, $Re = \rho_f U_p d_d / \mu_f$; and the Prandtl number, $Pr = \rho_f C_{pp} / \mu_f$. These were evaluated for arc plasma flowing over the droplet using plasma properties evaluated at a film temperature given by the following:

$$T_f = (T_p + T_{ds}) / 2 \quad [K] \quad (9)$$

For simplicity, the heat transfer coefficient was evaluated at one film temperature, $T_f = 6250$ K, and for the droplet diameter at detachment assuming no mass loss due to evaporation and a density evaluated at the initial droplet temperature. The film temperature of 6250 K was the mean of an assumed droplet temperature of 2500 K (approximately midway between alloy melting and boiling points) and an assumed plasma temperature of 10,000 K. Arc plasma temperature varies with position and current. Lancaster (Ref. 13) gives values of 6000 K for an iron vapor arc and 10–15,000 K for a 200-A argon arc. Ten thousand K is an approximation. Using properties evaluated for a film temperature of 8000 K resulted in a fall in predicted FFR of between 12 and 20%. This gives an indication of the sensitivity of the model to a change in film temperature. Plasma velocity was given by the following (Ref. 4):

$$U_p = 3809u_w \quad [m.s^{-1}] \quad (10)$$

This applied to a 1.2-mm (0.047-in.) mild steel welding wire. The equation used to relate N_u , Re , and Pr was (Ref. 12)

$$N_u = 0.37 Re^{0.6} Pr^{(1/3)} \quad (11)$$

This equation applies to forced convection for a gas flowing over a sphere. It is valid for $20 < Re < 150,000$.

Evaporation

Evaporation from the droplet was calculated from the convective mass transfer coefficient for each metal, k_{ci} , using the following equation:

$$E_i = \left(k_{ci} x_i P_i M_i \right) A_{ds} \left(1 / 100\omega \right) / (RT_{ds}) \quad [kg] \quad (12)$$

This equation approximates the situation by assuming metal vapor concentration in the plasma is small compared to vapor concentration at the droplet surface and, so, can be taken as zero. As in the Dennis Model, only Fe and Mn evaporation were considered. Evaporation of Si and trace elements found in mild steel were ignored. $x_i P_i$ represents the vapor pressure of element i and is the product of mass fraction i in the droplet and pure vapor pressure i at temperature T_{ds} . Strictly speaking, the mole fraction for the element, rather than the mass fraction, should have been used, but since the atomic masses of Fe and Mn are similar and these two elements make up the majority of the welding wire, then mass and mole fractions were very similar. It was assumed in calculating the change in composition of the welding wire that the other elements found in small amounts in the welding wire remained at the same mass fraction values. Representing the vapor pressure using $x_i P_i$ assumes an activity coefficient equal to one. The Langmuir equation for comparison is

$$E_i = X_i P_i A_{ds} \left(\frac{M_i}{2\pi RT_d} \right)^{0.5} \left(1 / 100\omega \right) \quad [kg] \quad (13)$$

Pure vapor pressures were calculated using the Dennis Model equations, which

represent curve fits to National Physical Laboratory data.

$$\text{Log } P_{Fe} = 10.41682 - 15724 / T_{ds} - 3930000 / T_{ds}^2 \quad \left[N.m^{-2} \right] \quad (14)$$

$$\text{Log } P_{Mn} = 9.50342 - 9246 / T_{ds} - 2940000 / T_{ds}^2 \quad \left[N.m^{-2} \right] \quad (15)$$

To obtain k_{ci} values, it was necessary to calculate the Sherwood number, $Sh = k_c d_d / D_{AB}$. In this case, the Frössling equation (Ref. 12), which follows, was used.

$$Sh = 2.0 + 0.552 Re^{(1/2)} Sc^{(1/3)} \quad (16)$$

The equation is valid for $2 < Re < 800$ and $0.6 < Sc < 2.7$, where the Schmidt number, $Sc = \mu_f / (\rho_f D_{AB})$. D_{AB} is the mass diffusivity of A through B and was evaluated for Fe and for Mn diffusing through the shielding gas mixture given in Table 3. For simplicity, k_{cFe} and k_{cMn} were evaluated for plasma properties at a film temperature of 6250 K and for the droplet diameter at detachment assuming no mass loss due to evaporation and a density evaluated at the initial droplet temperature.

Evaporation Energy Transfer

Once the evaporation mass loss over a given time increment was determined, the energy loss due to the latent heat of vaporization could be calculated as follows.

$$Q_{Evap} = E_{Fe} H_{vFe} + E_{vMn} H_{vMn} \quad [J] \quad (17)$$

Forming Droplet

Due to the droplet increasing in size as it grows, heat transfers by radiation, con-

Table 4 — Selected Calculated Quantities Using the New Model

| Experiment Test | Predicted Arc Length [mm.(in.)] | Fe Evaporation Rate [kg.s ⁻¹] | Mn Evaporation Rate [kg.s ⁻¹] | Fraction Metal Vapor to Fume | | Reynolds Number R _e | Fe Mass Transfer Coefficient k _{Fe} [m.s ⁻¹] | Mn Mass Transfer Coefficient k _{Mn} [m.s ⁻¹] |
|--------------------|---------------------------------------|--|--|------------------------------------|-------|--------------------------------------|--|--|
| | | | | Fe | Mn | | | |
| 1 | 6.1 (0.240) | 2.63E-05 | 4.87E-06 | 0.052 | 0.051 | 306 | 16.1 | 16.1 |
| 2 | 3.4 (0.134) | 2.27E-05 | 4.62E-06 | 0.066 | 0.064 | 285 | 19.9 | 19.9 |
| 3 | 4.4 (0.173) | 2.38E-05 | 5.07E-06 | 0.066 | 0.064 | 308 | 22.7 | 22.8 |
| 4 | 7.4 (0.291) | 2.80E-05 | 6.04E-06 | 0.056 | 0.053 | 378 | 23.1 | 23.2 |
| 5 | 5.0 (0.197) | 2.40E-05 | 5.81E-06 | 0.056 | 0.054 | 432 | 25.3 | 25.3 |
| 6 | 6.2 (0.244) | 2.58E-05 | 6.22E-06 | 0.054 | 0.052 | 444 | 26.3 | 26.4 |
| 7 | 7.8 (0.307) | 2.81E-05 | 6.91E-06 | 0.048 | 0.046 | 525 | 26.7 | 26.7 |

Table 5 — Fume Composition

| Current [A] | Experiment | | Current [A] | Predicted | |
|----------------|----------------|----------------|----------------|----------------|----------------|
| | Fe [mass %] | Mn [mass %] | | Fe [mass %] | Mn [mass %] |
| 180 | 59 | 7.9 | 175 | 55.1 | 9.9 |
| 205 | 56 | 9.4 | 188 | 54.3 | 10.7 |
| 220 | 57 | 8.9 | 212 | 53.9 | 11.1 |
| 240 | 57 | 7.0 | 240 | 53.8 | 11.2 |
| 260 | 58 | 6.4 | 256 | 52.8 | 12.2 |
| 268 | 59 | 6.6 | 269 | 52.8 | 12.2 |
| 300 | 61 | 6.4 | 294 | 52.6 | 12.4 |

vection, droplet resistance heating, and evaporation change. Temperature of the droplet also changes. Over each time increment, energy and mass transfers were calculated and used to adjust the droplet temperature and composition at the beginning of the next time period. This process was repeated until the droplet detached from the welding wire at time $1/\omega$.

Falling Droplet

Once the droplet detached from the welding wire tip, it fell across the arc, accelerated by the plasma jet drag force and gravity. During the falling stage, the droplet was no longer receiving mass from the welding wire. Electron condensation and resistance heating ceased since zero current flow through the detached droplet was assumed. Only radiation, convection, and evaporation were considered. Mass and energy balances were conducted over small time increments to obtain droplet temperature, mass, and composition changes with time. Droplet falling time was estimated by calculating the drag force on the detached droplet as follows:

$$F_d = f A_{dp} \rho_f U_p^2 \quad [N] \quad (18)$$

where $U_p = 3809u_w$ as used previously and f is a dimensionless friction factor, which can be expressed as the following function

of R_e , valid for $0.2 < R_e < 800$ (Ref. 14):

$$f = 12 \left(1 + 0.15 R_e^{0.687} \right) / R_e \quad (19)$$

Droplet acceleration is drag force divided by mass plus acceleration due to gravity. The falling time was calculated, as follows, assuming constant acceleration.

$$t_{fall} = \left(2L_a m_d / (F_d + m_d g) \right)^{0.5} [s] \quad (20)$$

Plasma properties were evaluated for a film temperature of 6250 K and used to calculate f and F_d . Mass and diameter of the falling droplet were calculated assuming no loss by evaporation and a temperature of T_d (initial). A time increment of $t_{fall}/100$ was used for the falling time calculations. The arc length was derived from electrode extension, which was estimated using an equation from Halmøy (Ref. 9) for wire velocity valid for $H_1 > 4 \times 10^9 \text{ J.m}^{-3}$ and for Union K56 Si-M steel solid welding wire. The equation was rearranged as given below:

$$L = u_w \left(15.1 \times 10^9 - 3.5 j_w \right) / \left(1.2 \times 10^{-6} j_w^2 \right) \quad [m] \quad (21)$$

Arc length was obtained by subtracting electrode extension from standoff (assumes base of arc level with base metal surface).

Metal Vapor Generation Rate and Fraction Condensed on Base Metal

The results of the above calculations, performed using a computer spreadsheet program, included T_{ds} , x_{Fe} , and x_{Mn} as functions of time. Mass Fe and Mn evaporated can be evaluated from droplet composition, welding wire feed rate, and welding wire composition. Multiplying total mass of metal evaporated from one droplet by the droplet rate gave the metal vapor generation rate (M_{VGR}). Not all of this is thought to form fume. Haidar (Ref. 6) calculated 85 to 95% of the evaporated metal comes into contact with the base metal; most would be expected to condense. Parameters used were 1.6-mm-diameter (0.063-in.) mild steel welding wire at 300 A, pure argon shield, 8-mm (0.315-in.) initial arc length, 24-mm (0.945-in.) welding wire extension, and $1.67 \times 10^{-2} \text{ m}^3 \cdot \text{s}^{-1}$ gas flow rate. The Dennis Model used an average value of 90% condensed in the calculations for FFR. The New Model used the Deam Model method. In this method, vapor condensation on the base metal was estimated assuming potential flow. The resulting equation relating rate of metal vapor entering fume (M_{FFR}) to M_{VGR} was

$$M_{FFR} = M_{VGR} \left(1 + M_{VGR} / 2\alpha \right)^{-1} \quad [kg.s^{-1}] \quad (22)$$

$$\alpha = U_o \pi \left(I_{mix} \right)^2 \rho_v \quad [kg.s^{-1}] \quad (23)$$

The equation was evaluated separately for Fe and Mn. The metal vapor density for element i , assuming ideal gas behavior, was given by the following:

$$\rho_{vi} = M_i x_i P_i / (RT_{ds}) \quad [kg.m^{-3}] \quad (24)$$

Using this method, the fractions of metal condensed for Fe and Mn vapors were calculated separately and applied to the

metal evaporation results to give values for the total M_{FFR} . GMAW fume contains oxidized metal and is typically 65% metal with the remainder mainly oxygen. M_{FFR} values were multiplied by 100/65 to give predicted FFRs.

Results and Discussion

Calculations were performed on the experimental data set given in Table 3, which covers the globular to spray transition region and full spray region. Table 4 gives a selection of calculated quantities using the New Model.

FFR Predictions

Explanation of Figure 1

Figure 1 shows FFR against current taken from Ref. 5 with the New Model FFR predictions added.

In the legend, "experimental" points are those obtained by A. D. Workman (Ref. 5) for which arc length was controlled to 5 mm (0.197 in.) and droplet rate was measured. "Additional" points were FFR measurements done by other workers under conditions close to those used by Workman, but without arc length controlled to 5 mm (0.197 in.). The "additional" points give a better idea of the shape of the FFR current curve and the variation in measured FFR at a particular current. In preparing this paper, it was discovered the typical wire composition given in Ref. 5 was incorrect according to analysis by the wire manufacturer. Mn was given as 1.2% whereas 1.4% is a more correct figure. The Dennis Model predictions in Fig. 1 were calculated using the value of 1.2% Mn and the same liquid metal density equation as used in the New Model. Using a value of 1.4% Mn would give a maximum increase in Dennis Model predicted FFRs of less than 8%.

Predictions

The New Model predicts approximately constant FFR with values less than experimental measurements in the low and high current regions. The Dennis Model is a better predictor except for the prediction at 240 A. Since neither model includes contributions to fume from processes other than evaporation from droplets, the predicted FFRs would be expected to be less than experimental rates.

Tapering in Spray Region

The divergence between the New Model predictions and experimental values at the higher currents may be partly due to the effects of electrode tip taper-

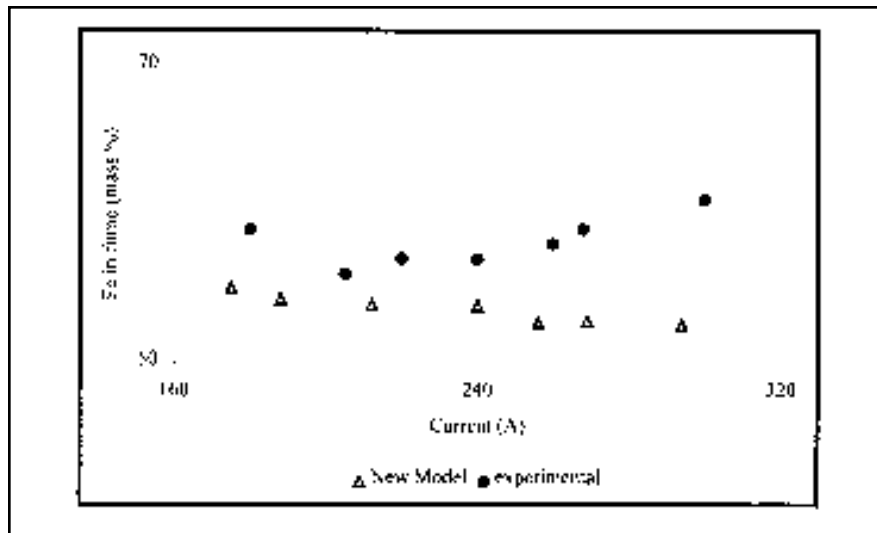


Fig. 4 — Fe concentration in fume estimated using the New Model compared with experimental values obtained under similar conditions.

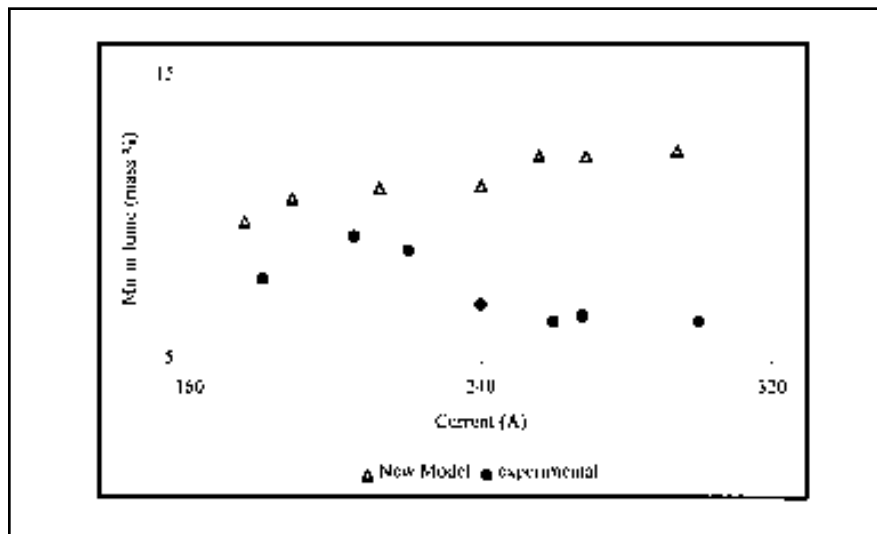


Fig. 5 — Mn concentration in fume estimated using the New Model compared with experimental values obtained under similar conditions.

ing, which occurs in the spray transfer region. As a result, the area of molten metal is greater than that predicted assuming a simple spherical droplet shape. Photographic evidence (Ref. 15 and Ref. 7 [for aluminum]) indicates in spray transfer, the arc envelope extends up the taper, whereas in globular transfer, it is largely confined to the droplet and region extending to the base metal. The taper gives greater area for radiation and convection energy transfer from the arc and greater area for evaporation than predicted by the simple spherical droplet model used here. Surprisingly, the Dennis Model results, also obtained using a spherical

droplet model, give reasonable agreement with experimental results in the spray region. Droplet shape and area and the effect of electrode tapering could be better modeled. Detailed data from experimental observations and measurements would aid in that. For an analysis of liquid flow and heat transfer at the wire tip in spray transfer, see Waszink and Van Den Heuvel (Ref. 16)

Effect of Using Halmøy Equation

One major difference between the two models was the New Model used arc lengths (Table 4) estimated using the

Halmøy equation for wire velocity (Ref. 9) rearranged to give electrode extension as a function of wire velocity (Equation 21). The New Model results were reevaluated using a constant arc length value of 5 mm (0.197 in.), as used in the Dennis Model. Figure 2 shows the resulting FFRs, which demonstrate improved prediction. It appears the use of the Halmøy equation was a major source of the difference between our predictions and those from the Dennis Model. The equation for wire velocity was applicable to Union K56 Si-Mn steel. A more valid calculation would need further experiments to determine the constants in the equation for the specific wire used in the Dennis Model experiments. In deriving the equation, Halmøy took the heat content per unit volume of the droplet at detachment as being the sum of the resistance heating in the wire and the effective anode heating. Halmøy compared his equation with an approximation of an equation from Lesnewich (Ref. 17) and concluded the heat content at detachment was constant. Detaching droplets having a constant specific heat content is inconsistent with the change in detachment temperature with current predicted here. Halmøy did not take into account evaporation, convection, or radiation. Further study is necessary to find out the reasons for the inconsistency.

Temperature Predictions

Figure 3, based on Ref. 5, shows temperature predictions for droplets as they start to form (initial), when they detach from the wire tip (detachment), and when they enter the weld pool (final). Dennis Model predictions were calculated using corrected wire composition and a liquid metal density equation as used in the New Model. The New Model predictions gave much higher temperatures because surface temperature values were used as opposed to mean temperature values. New Model initial temperatures were in excess of alloy boiling point and fell with increasing current. Interestingly, New Model detachment temperatures were roughly constant at around the alloy boiling point (approximately 3100 K). This may be connected with using the Halmøy equations. Final temperatures were approximately 200 K lower. Villemint (Ref. 18) measured surface temperatures of droplets and found values ranging from 2600 to 3100 K, which are comparable with New Model predictions for droplets at the detachment and final stages.

Fume Composition

Fume composition in terms of Fe and

Mn concentrations can be estimated from the ratio of M_{FFR} values for Fe and Mn. The calculations use the assumption of a constant Fe+Mn content for the fume of 65% (GMAW fume is typically 65% metal). Table 5 compares predicted compositions with experimental compositions obtained under conditions that were similar but not identical. Figures 4 and 5 show these results in graphical form. Fe concentration is underestimated and Mn concentration overestimated with divergence between experimental, and predicted values increasing at the higher currents. Droplet surface temperature largely determines the predicted ratio of Fe to Mn in fume. As the temperature of an alloy of Fe and Mn increases, the ratio of the equilibrium vapor pressure of Fe to Mn increases, hence vapor composition becomes richer in Fe and leaner in Mn. Complete evaporation of microdroplets resulting from gas bubble burst and other mechanisms would result in a fume richer in Fe. If mixing in the droplet was insufficient to supply Mn to the surface as fast as it was evaporating, then Mn depletion at the surface would occur, which could also result in a fume richer in Fe. In one study involving pulse welding, depletion was not found except at high oxygen concentrations (20%) (Ref. 19). In the Method section of this paper, mention was made of oxidation-enhanced evaporation and how it was less for Mn than for Fe. If oxidation-enhanced evaporation was taking place, it might account for differences between experimental and predicted compositions. Formation of FeO and MnO on the droplet surface would have an effect on evaporation rates. Further study of oxidation and evaporation processes occurring at the droplet surface would help to establish the validity of a simple metal evaporation model.

Shielding Gas Effects

Shielding gases used in mild steel GMAW normally contain oxygen and/or carbon dioxide. Carbon dioxide can be a source of oxygen at high temperatures. The presence of oxygen may result in oxidation-enhanced evaporation from droplets. This was assumed in the Dennis Model, but no account was taken of varying oxygen concentration effects. Studies have found an increase in oxygen concentration in shielding gas can lead to increased FFR (Refs. 20, 21). Shielding gas composition can also affect droplet rate. Oxygen in low concentrations enhances spray transfer by lowering surface tension of the droplets. Droplet rate is one of the inputs to the model, which is not a normally measured quantity in continu-

ous current commercial welding situations. A method to predict droplet rate from normally measured parameters is one requirement for an improved model. Shielding gas flow rate influences predicted FFR in the New Model due to its effect on the proportion of metal vapor condensed to the base metal. Experiments at different shielding gas flow rates would enable a comparison of the predicted effect with the experimental effect. A comprehensive FFR model would have to incorporate shielding gas composition and flow rate effects on FFR. The New Model used gas physical property data estimated for the shielding gas composition used in the experimental work. The New Model was also run using physical property data estimated for CO₂ and the predicted FFR was found to increase by 16 to 22%.

Conclusions

- The New Model has addressed certain points raised in Ref. 5 concerning the Dennis Model. It has replaced the Langmuir evaporation assumption with a mass transfer correlation. It has included the effects of radiation and convection energy transfers. It has calculated droplet falling time in place of using an equation derived from indirectly applicable experimental data. It has calculated condensation based on system conditions in place of using a constant approximate value. It has replaced measurement of arc length with a method to calculate arc length. The result has been a more theoretically based model that is not as good as the Dennis Model in predicting FFR and that predicts initial surface temperatures in excess of the boiling point.
- Improvement of the model to account for the effects of tapering of the welding wire tip in the spray region may improve predictions, although the Dennis Model gave reasonable predictions for the spray region despite using a simple spherical droplet model.
- The use of the Halmøy equation for wire velocity to estimate arc length was one major source of difference between the models. Further study would be necessary to improve this part of the model.
- The New Model allows estimation of fume composition (as did the Dennis Model). It underestimates Fe concentration and overestimates Mn concentration. Divergence between experimental and predicted values increases at the higher currents.
- The New Model incorporates calculation of fraction metal vapor condensed

to the base metal. The fraction depends on shielding gas velocity and may be a partial explanation of observed effects of shielding gas flow rate on FFR.

Acknowledgments

Much of the content of this paper relies on work by Deam, Simpson, and Haidar (Ref. 4) and by Dennis, Hewitt, Redding, and Workman (Ref. 5). Figures 1-3 and Table 3 are taken, with changes, from Ref. 5 with the permission of the British Occupational Hygiene Society.

References

1. International Agency for Research on Cancer (IARC). 1990. Evaluation of carcinogenic risk to humans. Chromium, nickel and welding. *IARC* 49. Lyons, France.
2. Milatou-Smith, R., Gustavsson, A., and and Sjögren, B. 1997. Mortality among welders exposed to high and to low levels of hexavalent chromium and followed for more than 20 years. *Int. J. Occup. Environ. Health* 3(2): 128-131.
3. Beach, J. R., Dennis, J. H., Avery, A. J., Bromley, C. L., Ward, R. J., Walters, E. H., Stenton, S. C., and Hendrick, D. J. 1996. An epidemiological investigation of asthma in welders. *Am. J. Resp. Critical. Care. Med.* 154(5): 1394-1400.
4. Deam, R. T., Simpson S. W., and Haidar, J. 2000. A semi-empirical model of the fume formation from gas metal arc welding. *J. Phys. D: Appl. Phys.* 33: 1393-1402.
5. Dennis, J. H., Hewitt, P. J., Redding, C. A. J., and Workman, A. D. 2001. A model for prediction of fume formation rate in gas metal arc welding (GMAW), globular and spray modes, DC electrode positive. *Ann. Occup. Hyg.* 45(2): 105-113.
6. Haidar, J. 1999. An analysis of heat transfer and fume production in gas metal arc welding. *III. J. Appl. Phys.* 85(7): 3448-3459.
7. Needham, J. C., Cooksey, C. J., and Milner, D. R. 1960. Metal transfer in inert gas shielded arc welding. *British Welding Journal* (2): 101-114.
8. Turkdogan, E. T., Grieveson, P., and Darken, L. S. 1963. Enhancement of diffusion-limited rates of vaporisation of metals. *J. Physical Chemistry* 67(8): 1647-1654.
9. Halmøy, E. 1979. Wire melting rate, droplet temperature and effective anode melting potential. *Conference on Arc Physics and Weld Pool Behaviour*, pp. 49-57. United Kingdom: The Welding Institute.
10. Zacharia, T., David, S. A., and Vitek, J. M. 1991. Effect of evaporation on weld pool development. *Metallurgical Transactions B22B* (April): 233-241.
11. Metcalfe, J. C., and Quigley M. B. C. 1977. Arc and pool instability in GTA welding. *Welding Journal* 55(5): 133-s to 139-s.
12. Welty, J. R., Wilson, R. E., and Wicks, C. E. 1979. *Fundamentals of Momentum Heat and Mass Transfer*, 2nd ed. New York, N.Y.: Wiley.
13. Lancaster, J. F. 1987. *Metallurgy of Welding*, 4th ed. London, United Kingdom: Allen and Unwin.
14. Coulson, J. M., and Richardson, J. F. 1968. *Chemical Engineering* Vol. 2, 2nd ed., p. 140. New York, N.Y.: Pergamon Press.
15. Lesnewich, A. 1958. Control of melting rate and metal transfer in gas shielded metal arc welding: Part II: control of metal transfer. *Welding Journal* 37(9): 418-s to 425-s.
16. Waszink, J. H., and Van Den Heuvel, G. J. P. M. 1982. Heat generation and heat flow in the filler metal in GMA welding. *Welding Journal* 61(8): 269-s to 282-s.
17. Lesnewich, A. 1958. Control of melting rate and metal transfer in gas-shielded metal-arc welding, Part 1: control of electrode melting rate. *Welding Journal* 37(8): 343-s to 353-s.
18. Villeminot, P. 1966. Pyrometrie photographique appliquee au soudage. *Document 212-83-66*, International Institute of Welding.
19. Corderoy, D. J. H., Wills, B., and Wallwork, G. R. 1980. Gas/weld metal reactions in MIG arc plasma. *Conference on Weldpool Chemistry and Metallurgy*, pp. 147-153. United Kingdom: The Welding Institute.
20. Gray, C. N., Hewitt, P. J., and Hicks, R. 1980. The effect of oxygen on the rate of fume formation in metal inert gas welding arcs. *Conference on Weldpool Chemistry and Metallurgy*, pp. 167-176. United Kingdom: The Welding Institute.
21. Heile, R. F., and Hill, D. C. 1975. Particulate fume generation in arc welding processes. *Welding Journal* 54(7): 201-s to 210-s.